ELSEVIER

Polymer 41 (2000) 7147–7157

polymer

Structural changes in poly(ethylene terephthalate) induced by mechanical milling

C. Bai[a], R.J. Spontak[a], C.C. Koch[a], C.K. Saw[1,b], C.M. Balik*

[a]*Department of Materials Science and Engineering, Box 7907, North Carolina State University, Raleigh, NC 27695, USA*
[b]*Corporate Research Center, Hoechst-Celanese Corp., Summit, NJ 07901, USA*

Received 18 October 1999; received in revised form 29 December 1999; accepted 29 December 1999

Abstract

Poly(ethylene terephthalate) (PET) has been subjected to high-energy ball milling (mechanical milling, MM) at three different temperatures. The resulting milled powder is characterized by molecular weight measurements, differential scanning calorimetry and wide-angle X-ray scattering. Regardless of the initial degree of crystallinity or milling temperature employed, MM apparently yields an "oriented amorphous" PET morphology in which the PET chains are locally aligned but rotationally disordered. This conclusion is based on the persistence of the (100) peak in otherwise amorphous x-ray patterns from milled PET. Thermograms of milled PET exhibit a small, broad crystallization exotherm and a large melting endotherm. The unusually small crystallization enthalpy is attributed to the local orientation of PET molecules present in the oriented amorphous morphology. Only minor rotations and translations of oriented PET molecules are needed to put the chains into register and, hence, the crystalline state. Evidence is also presented to suggest that extended-chain crystals of PET are produced upon crystallization of mechanically milled PET.

Keywords: Poly(ethylene terephthalate); Mechanical milling; Crystallization

1. Introduction

Mechanical attrition—high-energy ball milling of powders—is a non-equilibrium processing method that has generated great interest in the past few years as a viable route to the physical synthesis of metastable materials. It can be used to modify materials by refining the microstructure, homogenizing the composition, extending solid solubility, creating metastable crystalline phases, or producing metallic glasses [1]. Mechanical alloying was first developed by Benjamin and co-workers in the late 1960s as a means to produce complex oxide dispersion-strengthened (ODS) alloys [2]. The discovery [3] in 1983 that solid-state amorphization could be achieved by mechanical attrition stimulated its use as a non-equilibrium processing tool to produce metastable structures such as amorphous alloys, extended solid solutions, metastable compounds, nanocrystalline materials and quasicrystalline materials. It is convenient to divide mechanical attrition into two categories: "mechanical alloying" (MA), in which dissimilar elements or compounds are alloyed at the atomic or molecular level, and "mechanical milling" (MM), in which the structure or microstructure of single-component powders can be transformed by defects introduced through milling-induced deformation.

For metallic materials, the mechanism of MM is generally regarded as a combination of two competing processes: fracturing and cold-welding of powder particles. The same general mechanism is expected to hold for MM of polymers. However, some aspects of this mechanism may be different for polymers due to their chainlike molecular nature, lower moduli, and higher sensitivity to temperature. Mechanical milling could conceivably sever polymer molecules and consequently create free radicals, which may then react with other molecules in the system to produce crosslinks or grafts. Degradation of the polymer may occur due to the elevated local temperatures and possible chain scission produced during high-energy collisions between the milling balls. The low diffusivity of polymer molecules is expected to impede the cold-welding process [4]. The contribution of these various processes to the mechanism of MM of polymers has yet to be unraveled. In spite of these potential problems, several workers have

* Corresponding author. Tel.: +1-919-515-2126; fax: +1-919-515-7724.
E-mail address: balik@ncsu.edu (C.M. Balik).
[1] Lawerence Livermore National Laboratory, L-370, Livermore, CA 9450, USA.

0032-3861/00/$ - see front matter
PII: S0032-3861(00)00048-3

recently demonstrated that MM and MA can be used to produce polymers and blends with acceptable mechanical properties.

Shaw and co-workers first systematically investigated and applied MM to polymeric materials [5–13]. They found that milled polyamide could be consolidated at 100°C (160°C below the melting point), and that it exhibited greater hardness and compressive strength than melt-processed polyamide. While the milled polyamide showed lower ductility, its Charpy impact energy (80 J/m) was surprisingly greater than that of the melt-processed material (50 J/m). These data suggested that MM could be successfully applied to polymers. Later, MM was extended to other polymer systems. Ishida studied mechanically milled polyethylene, poly(tetrafluoroethylene), and a 50/50 blend of these two polymers [14], and reported that MM could (i) result in amorphization of crystalline polymers and (ii) induce formation of metastable crystal structures. Recent work by Castricum and co-workers on high-density polyethylene supported Ishida's conclusions and showed a complete transformation of the crystal structure from orthorhombic to the metastable monoclinic phase after MM [15]. However, Farrell et al. reported no change in crystallinity or crystal structure after 4 h of milling highly crystalline polypropylene [4].

The effect of MM on the molecular weight of polymers has been reported in some of the above investigations. Castricum et al. measured no change in the number-, weight-, or z-average molecular weight for polystyrene after 1 h of milling in a planetary mill [15]. They concluded that the milling energy was not sufficient to break the C–C bond. In contrast, Pan and Shaw [12] measured an increase in molecular weight, from 17,000 to 18,000 g/mol, after milling an acrylonitrile–butadiene–styrene terpolymer. It was not clear, though, whether this change was beyond experimental uncertainty. None of these previous investigations indicate that MM causes a reduction in polymer molecular weight, whereas recent efforts by Smith et al. [16] clearly show that poly(methyl methacrylate) can undergo a substantial decrease in molecular weight, depending on its pre-milled molecular weight and the milling temperature.

These preliminary studies have demonstrated the feasibility of conducting MM and MA with polymers, even though this technique has not yet been fully explored and the fundamental mechanisms operative during MM of polymers have not been elucidated. In a series of previous papers [17,18], we reported preliminary results obtained from MM of poly(ethylene terephthalate) (PET), and MA of PET with the aromatic thermotropic copolyester Vectra™. In this work, we present a more complete study of the effects of MM on PET molecular weight, crystallinity, and thermal behavior.

2. Experimental

2.1. Materials

Extruded PET was kindly provided by the Hoechst–Celanese Corporation (HCC). Two different grades were studied: a high-crystallinity fibrous PET and nearly amorphous PET pellets. These samples had crystallinities of 47 and 4% as determined by differential scanning calorimetry (DSC), and are hereafter referred to as "high-crystallinity" and "low-crystallinity" PET, respectively. The as-received materials were cooled to liquid nitrogen temperature and ground into small pieces using a commercial grinder, which produced no measurable changes in any PET properties. These samples are designated as "as-ground" PET.

2.2. Mechanical milling

High-energy ball milling was conducted in a SPEX 8000 shaker mill. The steel milling vial was loaded with 4 g of polymer and 40 g of steel balls (10 balls measuring 7.9 mm in diameter and 20 balls measuring 6.4 mm in diameter). In order to prevent oxidation during milling, the vial was sealed under argon after loading. Milling was conducted at three different temperatures, denoted as follows: (1) *ambimilling*, which refers to milling performed near ambient temperature (50°C) with a fan blowing air across the milling apparatus; (2) *coolmilling*, which refers to milling performed at a lower temperature (5°C) by blowing cold air from an air conditioner across the milling apparatus; and (3) *cryomilling*, which refers to milling performed near liquid nitrogen temperature (−180°C) by encasing the vial in a Teflon container through which liquid nitrogen could flow and contact the outer wall of the steel vial. In this work, low-crystallinity PET was ambimilled and cryomilled, while high-crystallinity PET was coolmilled only.

The temperatures specified above were measured from the external surface of the steel vial with a thermocouple while the mill was in operation. Local temperatures inside the vial cannot be measured during milling. Theoretical estimates of local temperature excursions occurring during impact of the milling media vary widely [19]. For metallic materials, typical values are several tens of degrees Celsius, with some models yielding values as high as 300°C[17]. Such estimates are unavailable for the case of milling of polymeric materials. The effect of such a temperature excursion is complicated by the viscoelastic nature of polymers and the instantaneous nature of impact events. The high shear rates encountered in a shaker mill would cause the polymer to behave as if it were at a lower temperature, according to time-temperature superposition principles. Thus, the high shear rates encountered during milling may offset somewhat the effect of any temperature excursions. For these reasons and from the thermocouple measurements noted above, we believe it is safe to presume that the local temperature of the polymer during ambimilling and coolmilling may be close to or slightly above the glass transition temperature (T_g) of PET (75°C), whereas the temperature of the polymer remains far below T_g during cryomilling. More accurate knowledge of this local temperature would not alter the conclusions reached in this paper.

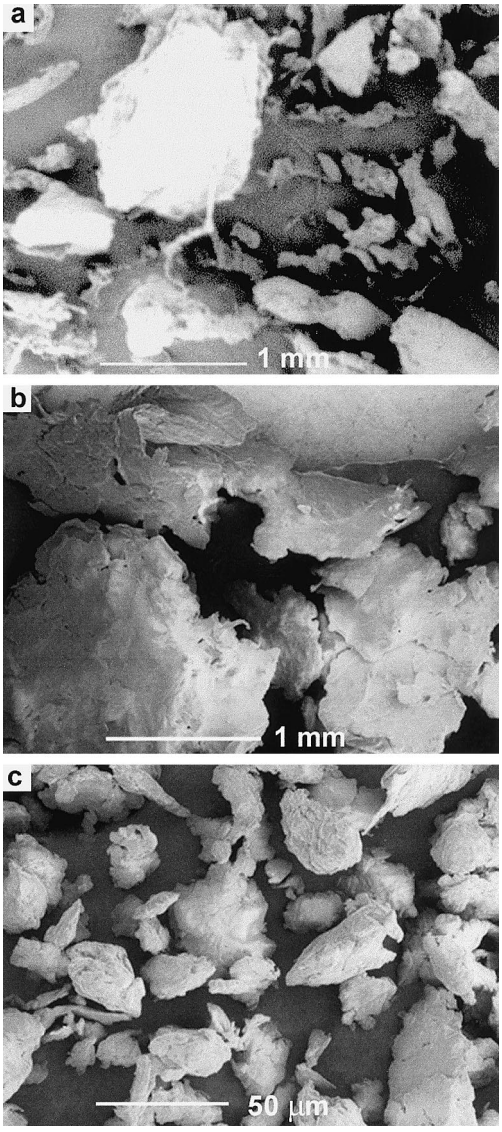

Fig. 1. Representative SEM micrographs of PET powder: (a) as-ground; (b) ambimilled for 20 min; and (c) ambimilled for 16 h.

2.3. Thermal properties

Differential scanning calorimetry (DSC) was performed on a DuPont 910 calorimeter at a heating rate of 20°C/min under an argon purge. The degree of crystallinity of PET before heating in the DSC (i.e. at ambient temperature) was calculated by subtracting the heat of crystallization from the heat of fusion and dividing by the heat of fusion for 100% crystalline PET (160 J/g) [20]. This was done in an attempt to remove the contribution of any crystallization occurring during the DSC scan, and to facilitate comparison of DSC crystallinities with x-ray diffraction data which were also collected at ambient temperature. It will be shown below that this DSC analysis can lead to erroneous conclusions about the as-milled crystallinity of PET. We therefore refer to the degree of crystallinity calculated in this manner as the "apparent" crystallinity.

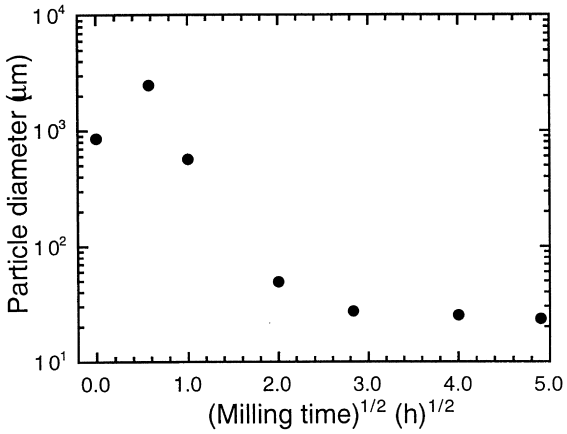

Fig. 2. Average particle size of ambimilled PET as a function of milling time. The particle size distribution in the as-ground material is very broad, but becomes narrower with increasing milling time (10:1 steel ball:polymer mass ratio).

2.4. Molecular weight

Molecular weights of milled PET were obtained from intrinsic viscosity measurements in *o*-chlorophenol at 25°C. As-prepared solutions were cloudy due to small amounts of SiO_2 additives, which were subsequently removed with 0.22 μm Millipore filters. The Mark–Houwink constants for these experimental conditions have been reported [21,22] as $K = 3.0 \times 10^{-4}$ dl/g (g/mol)$^{-a}$ and $a = 0.77$.

2.5. Morphology

Scanning electron microscopy (SEM) of gold-coated specimens was conducted on a JEOL 6400 field-emission microscope operated at 1.0 kV. Optical micrographs were obtained with a Nikon Optophot microscope equipped with a Hitachi CCD camera. Wide-angle x-ray scattering (WAXS) was performed at HCC using a Philips automatic powder diffractometer with a line source, and also at North Carolina State University with a Rigaku Geigerflex diffractometer equipped with a graphite monochromator. Both diffractometers employed Cu–K_α radiation.

3. Results

As-ground PET consists of roughly rounded particles which are flattened into flakes and then cold-welded together upon milling, as shown in Fig. 1 for ambimilled PET. Particle size distributions have been measured as a function of milling time from SEM micrographs, and the average size is plotted as a function of milling time in Fig. 2. Average particle sizes have been calculated from measurement of particle areas using the IMAGE software package from NIH, and conversion of average particle area to the diameter of an equivalent circle. The particle size initially increases with milling time as the rounded particles are

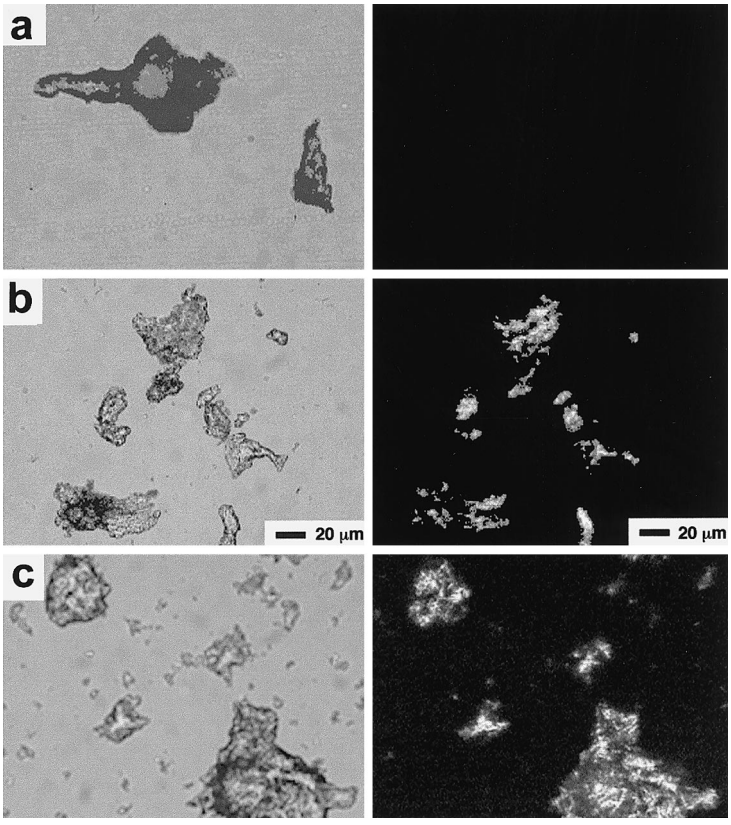

Fig. 3. Bright-field (left) and polarized (right) optical micrographs of low-crystallinity PET particles: (a) as-ground; (b) ambimilled for 16 h; and (c) cryomilled for 6 h. The scale bars in (b) apply to all Figs.

flattened into flakes and subsequently cold-welded together. After about 30 min of milling, the particle size decreases monotonically with milling time, leveling out at about 25 μm after 8 h of milling. The particle size distribution is very broad for the as-ground powder, but becomes considerably narrower with milling time. When the competing processes of cold-welding and particle fracturing reach a steady state, the microstructure can still be refined although the average particle size remains constant. The end product of MM is a fine powder with a distribution of particle sizes typically ranging from 10 to 40 μm, with a few particles as large as 70 μm. Fig. 1b clearly shows that the milled particles are flakelike and consist of an agglomeration of smaller flakes.

The compressive and shearing deformation that occurs during collisions between the steel balls is expected to produce biaxial stretching and orientation of the polymer chains within the powder particles. Displayed in Fig. 3 are bright-field and polarized optical micrographs of as-ground, ambimilled, and cryomilled PET powder. As-ground PET powder is not birefringent, whereas the milled powders are birefringent, which is consistent with the expectation that milling induces some degree of molecular orientation in PET.

The molecular weight of PET decreases for samples milled for 16 h, as shown by the data in Table 1. The percentage reduction is more significant for the ambimilled sample than for the coolmilled and cryomilled samples. Analysis of these samples by gel permeation chromatography (data not shown) reveals the same trend in number- and weight-average molecular weight, with no changes in the shape of the molecular weight distribution. Higher milling temperatures apparently induce a more pronounced decrease in PET molecular weight. This is not the expected result; chain scission upon particle fracture is thought to be more probable at low temperatures, whereas chain pullout upon particle fracture should be favored at higher temperatures. This conclusion, reached by Wool et al. [23,24], explains the effect of fracture temperature on the molecular weight of monodisperse polystyrene. They found that the number of chain scission events per unit area of fracture surface was

Table 1
Effect of mechanical milling on PET molecular weight

PET sample	Intrinsic viscosity (%)[a] (dl/g)	$\bar{M}_v$ (g/mol)	Percent change
Low crystallinity			
As-ground	1.138	44,500	–
Cryomilled 16 h	1.015	38,300	−13.9
Ambimilled 16 h	0.701	23,700	−46.7
High crystallinity			
As-ground	1.243	49,900	–
Coolmilled 16 h	1.054	40,300	−19.2
Coolmilled 35 h	1.029	39,000	−21.8

[a] Measured in *o*-chlorophenol at 25°C.

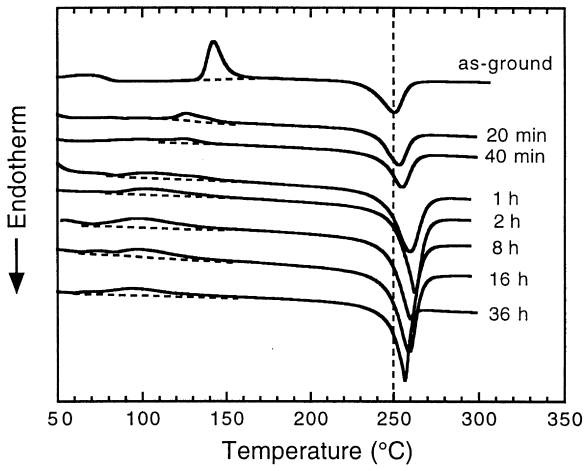

Fig. 4. DSC thermograms of low-crystallinity PET ambimilled for different periods of time.

significantly reduced at temperatures near T_g relative to temperatures well below T_g.

At this time, we can only speculate on the reasons for the effect of milling temperature on molecular weight. However, we have recently observed a similar but more dramatic reduction in molecular weight at higher milling temperatures for poly(methyl methacrylate) (PMMA) [16]. Thus, this effect does not appear to be peculiar to PET. If the energy from the milling process induces hydrolysis or some other chain scission reaction in PET, then the temperature effect on molecular weight might simply reflect reaction rate differences at these two temperatures. A slight yellowish discoloration has been observed for the ambimilled samples, while the cryomilled samples remained snow-white, which is strongly suggestive of the occurrence of oxidation or some other chemical reaction during ambimilling. It is also known that the activation energy required to break molecular bonds in polymers subjected to mechanical degradation is supplied by an external stress [24]. The normal thermal vibrations of the atoms comprising the chain augment this stress. Thus, for a given stress, it is possible for a bond to be stable at one temperature, but unstable at a higher temperature. This is a more general explanation for a milling temperature effect that is not strongly dependent on the polymer chemical structure, whereas the susceptibility of a polymer to certain chemical degradation reactions such as hydrolysis does depend on its chemical structure.

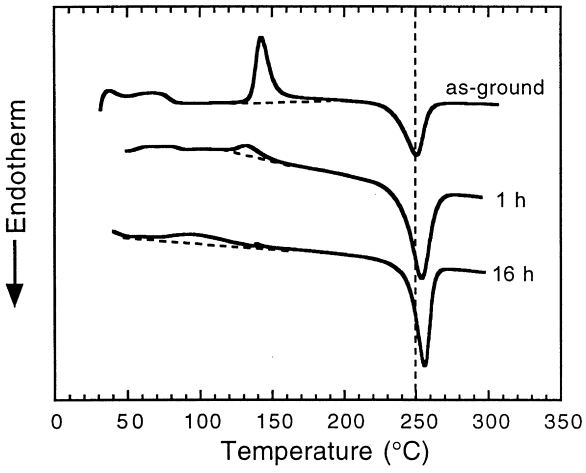

Fig. 5. DSC thermograms of low-crystallinity PET cryomilled for different periods of time.

Fig. 4 shows the DSC thermograms of low-crystallinity PET ambimilled for different periods of time. As expected, as-ground low-crystallinity PET exhibits a considerable crystallization exotherm at about 140°C. As milling time increases, the peak crystallization temperature decreases substantially (to about 100°C) in the early stages of milling and remains constant thereafter. The crystallization peak also becomes very broad and the corresponding heat of crystallization (peak area) decreases from about 25 J/g to less than 15 J/g. Meanwhile, the peak temperature for the melting endotherm (T_m) shifts to higher temperatures (10°C at most) with milling time and becomes sharper, with the heat of fusion increasing from 40 J/g to about 60 J/g. As seen before, most of these changes occur within the first hour of milling.

Cryomilling of low-crystallinity PET reveals similar behavior except that the changes proceed more slowly than for the ambimilled samples (see Fig. 5). Coolmilling of high-crystallinity PET shows somewhat different behavior (see Fig. 6). The crystallization exotherm is absent (as expected) for the as-ground sample, but appears as a broad, weak exotherm for the milled samples. Its behavior with milling time is similar to that of the low-crystallinity sample. The melting enthalpy of high-crystallinity PET decreases with milling time, whereas it increases with milling time for low-crystallinity PET. The melting peak temperature decreases slightly at short milling times, but then increases significantly at longer milling times. These data imply that the thermal properties of milled PET tend to be comparable regardless of the initial crystallinity of the material or milling temperature employed.

The peak melting temperatures (T_m) of the samples discussed in Figs. 4–6 are summarized in Fig. 7. In most cases, T_m for the milled samples is higher than T_m for the unmilled samples except for the high-crystallinity sample, which exhibits a slight decrease in T_m before increasing. The ambimilled low-crystallinity sample exhibits a larger increase in T_m than the cryomilled low-crystallinity sample. Other variations in T_m with milling time are evident in Fig. 7 for these samples, but the major consistent trend and point to be made from this data is that T_m increases for all samples after a sufficient amount of MM. We speculate that the increase in T_m for milled samples is an indication that MM followed by heating in the DSC produces more stable (i.e. extended-chain) PET crystals. This point is discussed further below.

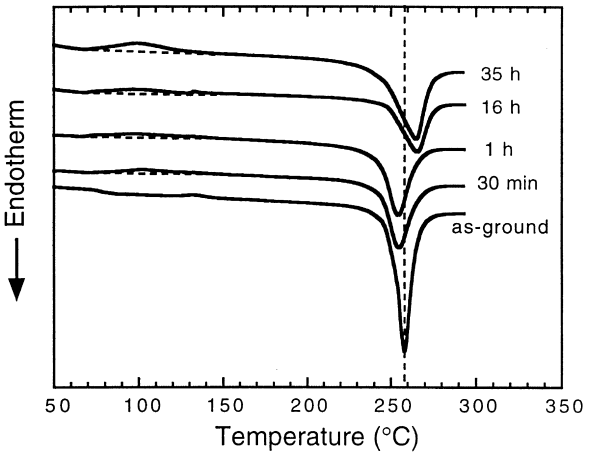

Fig. 6. DSC thermograms of high-crystallinity PET coolmilled for different periods of time.

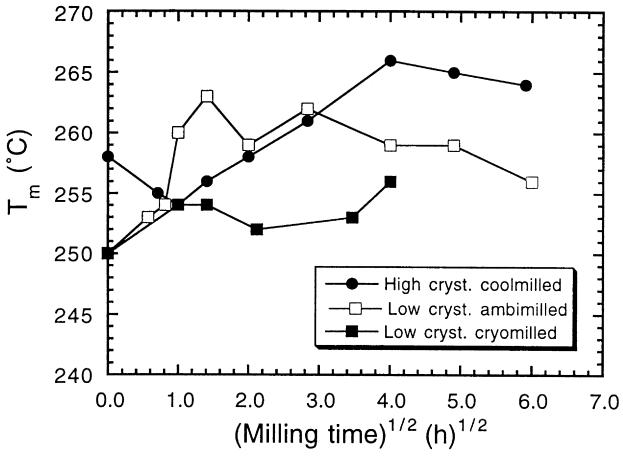

Fig. 7. Variation of peak melting temperature (T_m, from DSC measurements) with milling time for various PET samples and milling temperatures.

Apparent crystallinities for the samples in Figs. 4–6 are plotted against milling time in Fig. 8. In all cases, the apparent crystallinity changes significantly during the first hour of milling, after which time it attains a relatively constant value between 26 and 36%. The apparent crystallinities of all the samples fall into this range, regardless of the initial crystallinity of the sample or the milling temperature, and no significant difference in the behavior of the ambimilled and cryomilled low-crystallinity samples is evident. Also shown in Fig. 8 is the apparent crystallinity of a sample of low-crystallinity PET that was not milled but instead annealed at 190°C for various times. The rate at which the crystallinity of this sample increases is somewhat slower than that of the low-crystallinity milled samples, but the final crystallinity achieved again falls within the 26–36% crystallinity range. This indicates that MM and annealing at 190°C can produce about the same apparent crystallinity for amorphous PET after similar treatment times. Since the local temperature of the PET during milling is unlikely to exceed 190°C (especially during cryomilling), some mechanism other than thermal activation must be responsible for the more rapid increase in crystallinity for the milled PET compared to the annealed PET.

To explore the reversibility of the structural changes induced by milling, two samples of low-crystallinity PET, ambimilled 16 h and cryomilled 6 h, have been melted on a hot plate and then quenched into ice water. The DSC thermograms of these samples (not shown) exhibit the same features as those of the as-ground low-crystallinity PET shown in Figs. 4 and 5, confirming that changes induced by milling are primarily physical in nature and can be erased by appropriate thermal treatment.

X-ray scattering data provide additional insight into the effects of MM on PET at the molecular level. Wide-angle X-ray scattering patterns from coolmilled high-crystallinity

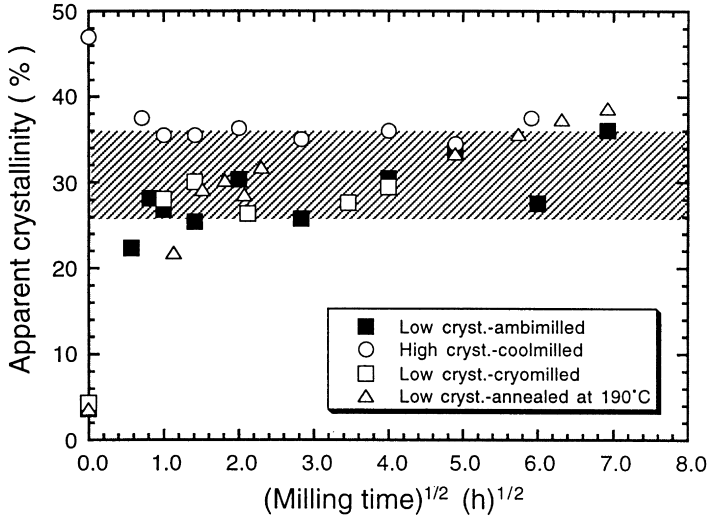

Fig. 8. Dependence of apparent crystallinity from DSC measurements for various PET samples and milling temperatures on milling time. Also shown is the apparent crystallinity for a quenched PET sample which was subsequently annealed at 190°C for various times.

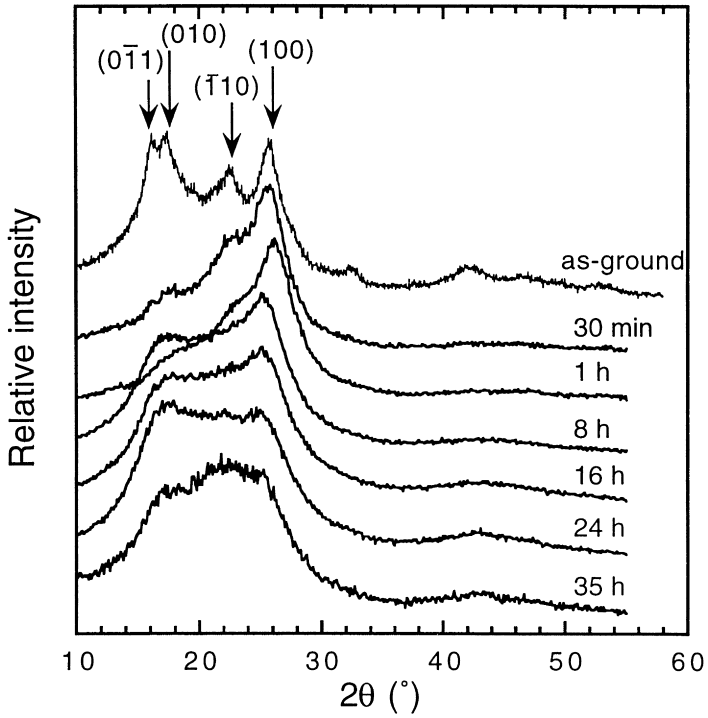

Fig. 9. WAXS patterns of high-crystallinity PET coolmilled for different periods of time.

PET are displayed in Fig. 9. During the first half-hour of milling, the (010) and ($\bar{1}$10) peaks disappear while the (100) peak remains. The (100) peak decreases in intensity with milling time and finally disappears after 24 h of milling. Fig. 10 shows the WAXS data for ambimilled low-crystallinity PET. The as-ground sample produces the expected amorphous pattern, whereas the scattering intensity at the Bragg angle for the (100) peak increases after ambimilling for 30 min. The WAXS pattern of PET after 16 h of ambimilling is similar to the 24-h pattern in Fig. 9. Fig. 11 shows that WAXS patterns from cryomilled low-crystallinity PET change very little after 16 h of cryomilling.

Comparison of Figs. 8 and 9–11 reveals that the degree of crystallinity of PET qualitatively deduced from WAXS is entirely inconsistent with the DSC measurements. The WAXS patterns of milled PET in Figs. 9–11 appear almost totally amorphous, but the DSC data from Fig. 8 indicate that the same PET samples have an apparent crystallinity of

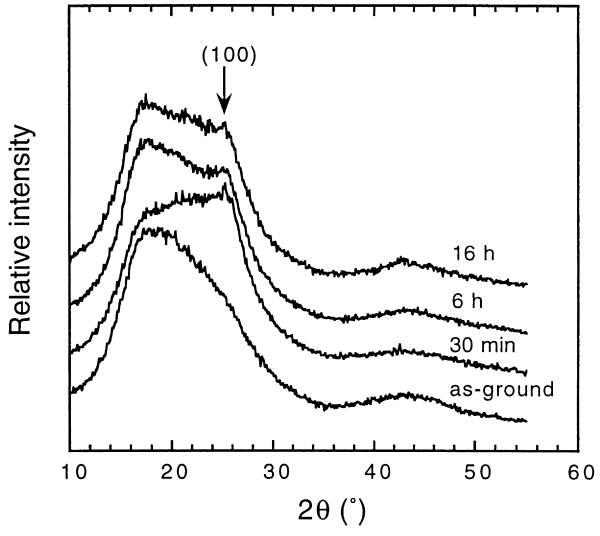

Fig. 10. WAXS patterns of low-crystallinity PET ambimilled for different periods of time.

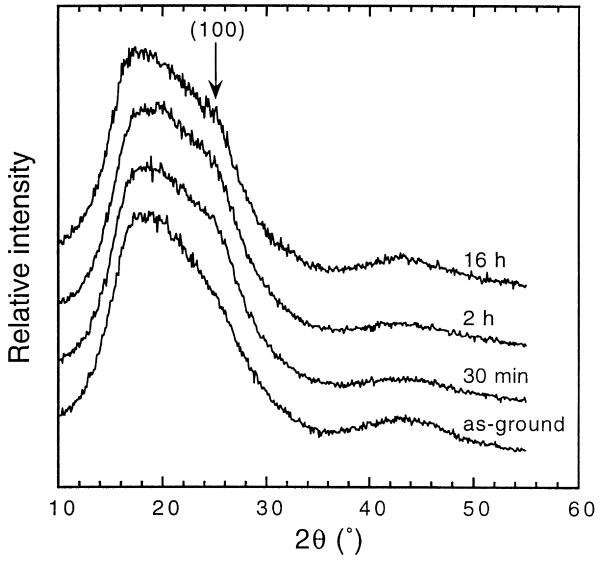

Fig. 11. WAXS patterns of low-crystallinity PET cryomilled for different periods of time.

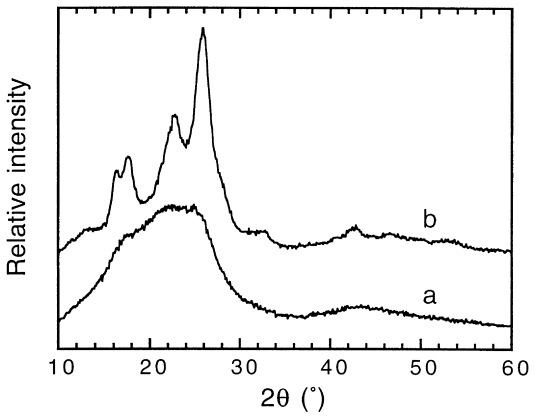

Fig. 12. WAXS patterns of low-crystallinity PET ambimilled for 16 h: (a) unannealed and (b) annealed at 200°C for 30 min. The apparent crystallinities obtained from DSC measurements were 30% for the unannealed sample and 38% for the annealed sample.

about 30%. This discrepancy suggests that crystallization of the milled samples occurs upon heating in the DSC, and is not accurately accounted for by subtracting the crystallization enthalpy from the fusion enthalpy, as described in Section 2. To prove this, samples of low-crystallinity PET ambimilled for 16 h have been annealed at 200°C for 30 min. This produced the highly crystalline WAXS pattern shown in Fig. 12, but the apparent crystallinity measured by DSC only increased to 38%. Thus, the high apparent crystallinity obtained for the milled (but unannealed) sample can be attributed to the abnormally small crystallization enthalpy evident in Figs. 4–6 for the milled samples. Further discussion of this point is provided in the next section.

4. Discussion

The PET unit cell is triclinic [26], and the phenyl rings in each PET molecule are nearly coplanar, as shown in Fig. 13. The phenyl rings are stacked on top of one another along the *a* axis of the unit cell, and are stacked side-by-side along the *b* axis. The WAXS patterns in Fig. 9 show that the (100) spacing (related to *a*) is more persistent during ambimilling of high-crystallinity PET than the (010) spacing (related to *b*). This would be expected on the basis of closer molecular packing and stronger van der Waals interactions along the *a* direction. Closer inspection of the patterns in Fig. 9 also reveals that the (100) peak shifts to slightly lower scattering angles for the 8- and 16-h ambimilled samples. This indicates that the spacing between the phenyl rings increases, which could result from some rotational disordering of the molecules about the chain axis during milling, while parallel alignment of the molecules is retained. Thus, we conclude that during the initial stages of MM, the PET crystals are disrupted via shearing parallel to the (010) planes, which destroys the (010) and $(\bar{1}10)$ spacings, while the stacking of

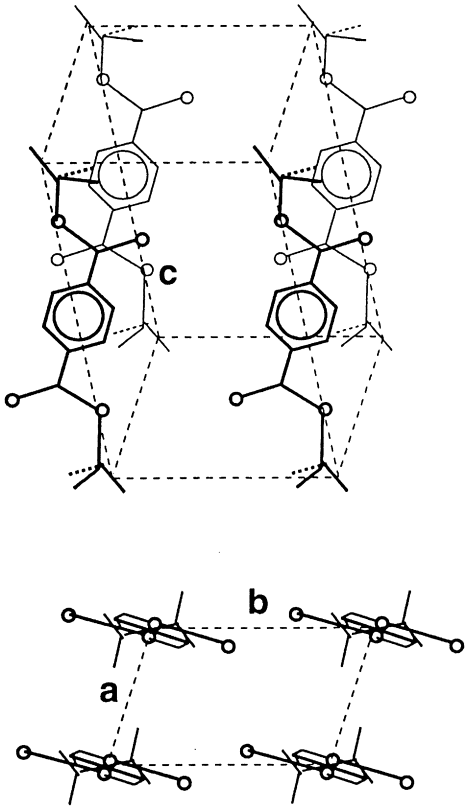

Fig. 13. Schematic diagram of the triclinic PET unit cell with $a = 0.456$ nm, $b = 0.594$ nm, $c = 1.07$ nm, $\alpha = 98.5°$, $\beta = 118°$, $\gamma = 112°$ (after Ref. [25]). Only two chains are shown in Fig. 12 for clarity.

molecules within the (010) planes (along *a*) persists. After 35 h of MM, this spacing is destroyed as well. Based on the persistence of the (100) peak, the morphology obtained between 1–24 h of MM consists of locally oriented but rotationally disordered PET molecules. We refer to this state as the "oriented amorphous" morphology. A similar microstructure, referred to as the "mesomorphic form", has been reported by Parravicini et al. [27] for cold-drawn amorphous PET fibers. Examples of oriented amorphous PET have also been recently observed by Asano et al. [30].

The PET molecules in the oriented amorphous morphology must be aligned in regions large enough to scatter x-rays coherently and give rise to the peak that is observed near the (100) position for the milled samples in Figs. 9 and 10. This requirement fixes the minimum size of these regions at several tens of nanometers, which is orders of magnitude smaller than the milled particle size, indicating that an individual milled particle may consist of many such regions (yielding a random overall chain orientation for each particle). Such macroscopically random orientation is consistent with the experimental observations that the milled particles consist of an agglomeration of smaller particles, and that the birefringence observed in Fig. 3 is not uniformly distributed throughout the particle. Instead, it corresponds to many small regions within each particle (see especially Fig. 3c). Thus, the existence of an oriented amorphous morphology

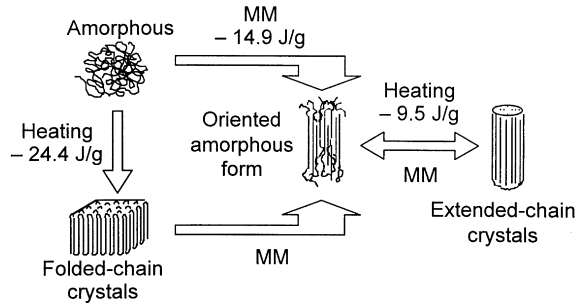

Fig. 14. Schematic illustration of the morphological changes presumed to occur in PET upon MM. Also shown are the enthalpies of transformation between the various states of PET from DSC measurements; see the text for a full description.

does not imply that macroscopic chain orientation persists throughout an entire milled particle, such as would result from cold-drawing of a PET fiber or thin film.

The same oriented amorphous morphology can likewise be produced by MM of initially amorphous (low-crystallinity) PET. This state is evidenced by the similar values of apparent crystallinity for the various PET samples after 1 h of milling (Fig. 8), as well as by the development of the peak near the (100) position in the WAXS patterns for milled low-crystallinity PET (Fig. 10). To produce this morphology, the polymer molecules must have sufficient mobility to align locally without fracturing. It is therefore not surprising that the development of the peak near the (100) position is much more pronounced during ambimilling than during cryomilling of low-crystallinity PET (compare Figs. 10 and 11). Recall that the local temperature inside the steel vial may exceed the T_g of PET during ambimilling, but the temperature inside the vial remains far below T_g during cryomilling, thereby impeding the ability of the PET molecules to align.

Fig. 12 verifies that annealing milled PET at 200°C for 30 min restores it to a highly crystalline state. While the same crystallization process probably occurs during heating of milled PET in the DSC, the crystallization exotherms in Figs. 4–6 appear to be too small to account for the amount of crystallization that takes place during heating. This leads to the large values of apparent crystallinity reported in Fig. 8 that are inconsistent with the corresponding WAXS patterns. The small enthalpy change accompanying crystallization of the milled samples can be explained in terms of the oriented amorphous morphology produced in PET by MM. The amount of heat released upon crystallization of milled PET is small because the oriented molecules are already very close to their final crystalline positions, and only need to undergo minor rotations and translations to enter into register. This transformation would be expected to produce a smaller enthalpy change relative to the change that accompanies the crystallization of quenched (unoriented) amorphous PET. As is evident in Figs. 4 and 5, quenched PET typically produces a crystallization exotherm comparable in magnitude to its melting endotherm. Moreover, Parravicini et al. [26] have reported DSC scans for their mesomorphic PET that appear very similar to the thermograms presented in Figs. 4–6 for milled PET. These thermograms exhibited a small, broad crystallization exotherm followed by an intense melting peak.

The observations presented here provide evidence for oriented amorphous PET and lead to the conclusion that crystallization of milled PET would be expected to produce extended-chain crystals rather than chain-folded crystals. Zachmann and Gehrke [28] studied the effect of chain orientation on the crystallization kinetics of PET using dynamic small angle X-ray scattering with synchrotron radiation. In their study, PET was oriented prior to crystallization either by drawing in the glassy state, by elongation during extrusion, or by imposing a shear gradient on the melt. They found that molecular orientation influences the rate of crystallization, the final degree of crystallinity, the ultimate morphology, and the crystal modification obtained. Prior orientation of the PET chains increased the rate of crystallization in all cases examined, whereas the opposite was true for melting. This trend was attributed to the preferential formation of extended-chain crystals over chain-folded crystals in PET oriented prior to crystallization. At the same temperature, a longer time was needed to melt oriented PET samples compared to unoriented samples. Therefore, during heating in a DSC at a fixed rate, the melting of oriented PET is expected to occur at a higher temperature compared to unoriented PET. Conversely, the crystallization of oriented PET measured at a fixed cooling rate should appear at a lower temperature compared to unoriented PET. Misra and Stein [29] also reported that extended chain crystals were formed upon annealing of cold-drawn amorphous PET at constant elongation (i.e. under stress), whereas annealing without an imposed stress produced chain-folded crystals.

The results of Zachmann and Gehrke [27] are in favorable agreement with the data presented here. The peak melting temperatures displayed in Figs. 4 and 5 for milled low-crystallinity PET are higher than those for as-ground PET by as much as 10°C (see also Fig. 7). The ambimilled samples have a higher T_m than the cryomilled samples, again implying that ambimilling induces a higher degree of chain alignment than cryomilling. Although the crystallization exotherms are rather broad in Figs. 4 and 5, it is clear that the crystallization temperature also decreases with milling time and is lower than that of as-ground PET.

The effects of MM on the PET structure can be summarized by the schematic illustration displayed in Fig. 14. Low-crystallinity PET has an unoriented amorphous structure. Heating this material in the DSC produces a well-defined crystallization exotherm and a melting endotherm having nearly the same magnitudes. The crystallization enthalpy for such PET is measured at −24.4 J/g. Since there was no prior orientation in the sample, chain-folded crystals develop. If this same sample is ambimilled for more than 1 h, the oriented amorphous morphology forms due to the

biaxial stresses inherent in the milling process. Because the sample is already oriented, much less heat is released upon crystallization in the DSC (about −9.5 J/g), and extended-chain PET crystals result. Knowledge of the enthalpies associated with these two processes, and assuming that the enthalpies associated with chain-folded and extended-chain crystals are similar, allows us to estimate the enthalpy of transformation from the unoriented amorphous to the oriented amorphous morphology, which we find is about −14.9 J/g. It follows that the majority of the enthalpy lost upon cold crystallization of PET comes from alignment of the molecules from a random coil state to a parallel oriented state, as would be expected. High-crystallinity PET may already exhibit an extended-chain crystalline morphology, or it may have a chain-folded morphology. In either case, MM disrupts the crystals and again produces the oriented amorphous morphology. As was the case for low-crystallinity PET, a low-crystallization enthalpy is observed when the microstructure crystallizes upon heating in the DSC.

This study not only provides evidence for intriguing amorphization and crystallization mechanisms in PET but also clearly demonstrates that using DSC alone to estimate the degree of crystallinity of PET (before heating in the DSC) can produce misleading results for samples that are highly oriented. Such crystallizable samples exhibit a low-crystallization enthalpy, which in turn translates into an erroneously high crystallinity when the crystallization enthalpy is subtracted from the melting enthalpy in the usual way. This pitfall can be avoided by using WAXS to qualitatively assess the crystallinity of the sample prior to DSC analysis.

5. Conclusions

Mechanical milling of PET powder results in a reduction of the average particle size from approximately 1 mm to 25 μm. The biaxial stresses experienced by the polymer during MM induce local orientation of the polymer molecules, and the milled particles become birefringent. The molecular weight of PET also decreases upon milling; this reduction is more pronounced for ambimilled compared to cryomilled PET. Apparent crystallinities measured by DSC increase with increasing milling time for PET initially having a low crystallinity, whereas high-crystallinity PET experiences a decrease in apparent crystallinity with increasing milling time. The apparent crystallinity of all samples falls within the range of 26–36% after about 1 h of milling, regardless of the milling temperature or the initial PET crystallinity. X-ray scattering patterns indicate that MM initially disrupts PET crystals by shearing parallel to the (010) planes, which leaves the intermolecular spacings along the *a* direction more or less intact. Sometime after 1 h of milling, the PET chains undergo rotational disordering about the chain axis and the intermolecular spacing along *a* is found to increase slightly. Extended milling produces an oriented amorphous morphology, regardless of the crystallinity of the PET sample before milling. The oriented amorphous morphology crystallizes upon annealing (or heating during DSC analysis) into extended-chain crystals, as evidenced by their higher melting temperature compared to unmilled PET. Since the polymer molecules in the oriented amorphous morphology are already close to their final crystalline positions, the heat of crystallization from this state is relatively small (about −9.5 J/g).

Acknowledgements

This work was supported by the Hoechst–Celanese Corporation and the Kenan Institute for Engineeering, Technology and Science at North Carolina State University. The authors wish to thank S. Lloyd, T. Malow and T. Smith for their assistance in milling and for performing some of the initial DSC and WAXS measurements.

References

[1] Koch CC. Mechanical milling and alloying. In: Cahn RW, editor, chap 5, vol. 15. Processing of metals and alloys, Cahn RW, Haasen P, Kramer EJ, editors. Materials science and technology—a comprehensive treatment, Weinheim, Germany: VCH Publishers, 1991: 194–245.
[2] Benjamin JS. Metall Trans 1970;I:2943–51.
[3] Koch CC, Cavin OB, McKamey CG, Scarbrough JO. Appl Phys Lett 1983;43:1017.
[4] Farrell MP, Kander RG, Aning AO. J Mater Synth Proc 1996;4:151.
[5] Pan J, Shaw WJD. Microstruct Sci 1992;19:659.
[6] Pan J, Shaw WJD. Proc 24th Int SAMPE Tech Conf, 1992, T762.
[7] Pan J, Shaw WJD. Microsruct Sci 1992;19:659.
[8] Pan J, Shaw WJD. Microstruct Sci 1993;20:351.
[9] Pan J, Shaw WJD. Microstruct Sci 1994;21:95.
[10] Pan J, Shaw WJD. J Appl Polym Sci 1994;52:507.
[11] Shaw WJD, Gowler MA. Proc First Int Conf Process Mater Prop TMS, Warrendale, PA, 1993:687.
[12] Shaw WJD, Pan J, Growler MA. Proc Second Int Conf Structural Appl Mech Alloying, Vancouver, BC, 1993:431.
[13] Shaw WJD. Polymer alloy material and process for production thereof, US Patent #5,367,048, November 1994.
[14] Ishida TJ. Mater Sci Lett 1994;13:623.
[15] Castricum HL, Yang H, Bakker H, Van Deursen JH. Proc Int Symp Metastable, Mechanically Alloyed and Nanocrystalline Materials, 1997:211, 235–8.
[16] Smith AP, Shay JS, Spontak RJ, Balik CM, Ade H, Smith SD, Koch CC. Submitted for publication.
[17] Balik CM, Bai C, Koch CC, Spontak RJ, Saw CK. Mater Res Soc Symp Proc 1997;461:39.
[18] Smith AP, Bai C, Ade H, Spontak RJ, Balik CM, Koch CC. Macromol Rapid Commun 1998;19:557.
[19] Koch CC, Int. J Mechanochem Mech Alloying 1994;1:56.
[20] Mehta A, Gaur H, Wunderlich B. J Polym Sci, Polym Phys Ed 1978;16:289.
[21] Ward IW. Nature 1957;180:141.
[22] Wallach ML. Die Makromol Chem. 1967;103:19.
[23] Wool RP, Rockhill AT. J Macromol Sci Phys B 1981;20:85.
[24] Willett JL, O'Connor KM, Wool RP. J Polym Sci Polym Phys Ed 1986;24:2583.
[25] Kausch HH. Polymer fracture. New York: Springer, 1987.

[26] Daubeny RDP, Bunn CW. Proc R Soc A (Lond.) 1954;226:531.
[27] Parravicini L, Leone B, Auriemma F, Guerra G, Petraccone V, Dino GD, Bianchi R, Vosa R. J Appl Polym Sci 1994;52:875.
[28] Zachmann HG, Gehrke R. Proc Int Meeting on Polymer Science and Technology, Limburg, The Netherlands, 1985:551.
[29] Misra A, Stein RS. J Polym Sci Polym Phys Ed 1979;17:235.
[30] Asano T, Calleja FJB, Flores A, Tanigaki M, Mina MF, Sawatari C, Itagaki H, Takahashi H, Hatta I. Polymer 1999;40:6475.